*Proc. of the 9th Intl. Conf. of Asian Society for Precision Engg. and Nanotechnology (ASPEN 2022)*
*15–18 November 2022, Singapore. Edited by* Nai Mui Ling Sharon and A. Senthil Kumar
doi://10.3850/978-981-18-6021-8_OR-15-0042

# A Fully Optical Laser Based System for Damage Detection and Localization in Rail Tracks Using Ultrasonic Rayleigh Waves: A Numerical and Experimental Study

**Faeez Masurkar[1,#], Fangsen Cui[1]**
[1]Institute of High-Performance Computing, A*STAR (Agency for Science, Technology, and Research) Research Entities, Singapore 138632, Singapore
[#]Corresponding Author / Email: masurkar_faeez_aziz@ihpc.a-star.edu.sg, TEL: +65-84387254

KEYWORDS: Rayleigh waves, Rail track, Optical system, Structural integrity, Damage localization, Non-Destructive testing.

*The present study focuses on investigating the structural integrity of rail track sections of the high-speed railways using the Rayleigh waves generated and sensed using a fully non-contact optical Laser system. The raw broadband beam of the excitation laser was converted to a narrowband beam using a customized optical system, whereas the propagating Rayleigh waves were sensed using a three-dimensional (3D) scanning laser Doppler vibrometer (3D-SLDV) system. All the experiments were conducted using the pitch-catch method in presence of surface damages on head of the Rail track. Several issues were observed during the experiments, which are noted as follows. First, the noise and unwanted wave packets increase with the increase in the time window and the inspection length. Second, with larger inspection lengths, it is relatively difficult to interpret the response as the reflection of the incident wave packet may arise from any edge of the rail specimen, and shall be difficult to precisely identify the source. Third, as a result of lower Signal-to-Noise ratio (SNR), there may be smaller wave packets that shall be likely deceiving as a reflection of the defect. Fourth, it is observed that a small change in the location of the sensing point may significantly alter the overall signal. Fifth, it is also observed that the actuation and sensing position plays a crucial role in receiving the time-domain data with a sufficient SNR and the one that is easy to analyze and interpret. Based on the numerous experiments, an optimum distance of inspection is estimated which yields damage detection and localization with high accuracy thereby solving all the aforementioned issues. Further, As the quality of received signals differs at different sensing points as a result of the surface conditions of the specimen, the Self Adaptive Smart Algorithm (SASA) method was adopted to filter out the noise and accurately pinpoint the defect reflected wave packet which ultimately aids in better detection and localization. Finally, a 3D Finite Element simulation was conducted to validate the findings and each observation resulting from the experiments. Based on the obtained accuracy of the results, the proposed methodology has been found to be capable of inspecting rail track specimens in a completely non-contact manner with reasonably good accuracy.*

**NOMENCLATURE**

$C_R, C_L, C_T$ = Rayleigh, Longitudinal, Transverse wave velocity;
$\lambda, \mu$ = Lame's constants; $\nu$ = Poisson's ratio of material
$\rho$ = Material density; $E$ = Modulus of Elasticity
$I^R$ = Incident Rayleigh wave; $I_d^R$ = Damage reflected Rayleigh wave; $\lambda_R$ = Wavelength of Rayleigh wave

## 1. Introduction

In this study, a fully non-contact optical system has been proposed for detection of surface damages in rail heads. High speed railways are gaining increasing attention worldwide as being effective and a timely means of transportation. However, the rail tracks may be subjected to constant and fluctuating loads over different times of service which may result in development of micro and macro scale damages in the rail material especially over the surface. This may consequently decrease the load bearing capacity of the rail track and eventually may result in failure and de-railing resulting into loss of economy and human life [1-2].

There are several techniques available to inspect rail damage such as visual, conventional non-destructive testing (NDT) techniques, and non-contact laser ultrasound-based scanning techniques. The majority of the inspection is yet accomplished with visual inspection technique that is rather labor intensive and often time consuming. For long range inspections, vehicles equipped with visual cameras and laser

scanning devices have been developed and commercialized. However, vision-based devices can only be able to detect surface damages and may also be affected by the outside weather conditions whereas laser-based ultrasound induced scanning can not only help detect surface damages but also the embedded damages [3-5].

The paper is organized as follows. First, the background and material description are given in Section 2. The details on the experimental and numerical study are given in Sections 3 and 4 respectively. The results are discussed in Section 5. Finally, the concluding remarks are given in Section. 6.

## 2. Background and Material description

In the present study, Rayleigh waves are excited and sensed using a fully non-contact laser transduction system and its fundamental background is given in the following sub-section.

### 2.1 Rayleigh waves

Rayleigh waves are the type of surface elastic waves that have a dominant particle motion near the surface of the solids, and they have both longitudinal and transverse particle motions. The energy of Rayleigh waves decrease exponentially in amplitude as the sensing point moves away from the surface. The governing equation of a Rayleigh surface wave is given as follows [5],

$$\eta^6 - 8\eta^4 + 8\eta^2(3 - 2\zeta^2) + 16(\zeta^2 - 1) = 0, \quad [1]$$

where,

$$\zeta = \frac{C_T}{C_L} = \sqrt{\frac{1-2\nu}{2(1-\nu)}} \quad [2]$$

and $\eta = \frac{C_R}{C_T}$. The approximate solution of $\eta$ is $(0.87 + 1.12\nu)/(1 + \nu)$. Thus, the Rayleigh wave velocity can be calculated as,

$$C_R = \left(\frac{0.87+1.12\nu}{1+\nu}\right) C_T, \quad [3]$$

From Eq. [3], it is clear that the Rayleigh wave velocity is independent of the frequency $f$, and thus they are non-dispersive. The material properties of the test specimen are given in following sub-section.

### 2.2 Material properties of test specimen

The specimen used for the study is a section of real rail track of the high-speed train as shown in Fig.1. The specimen received were in a pristine condition, however, all specimens had a significant amount of natural rust on their surfaces. Therefore, all specimens were polished before employing them for the experimental study. Initially a hand grinder was used to remove the rust and later a fine sandpaper was used to improve the surface quality of specimen. In particular, the surface portion of the rail track is always rust-free as it is in contact with the wheels of the train. This helps to acquire the wave propagation data with a higher signal-to-noise ratio (SNR). The mechanical properties of the specimen under investigation are given in Table.1

Table 1 Mechanical properties of the Rail track specimen [5]

| Mechanical properties | Value |
|---|---|
| $\rho$ (kg/m$^3$) | 7799 |
| $E$ (GPa) | 212 |
| $\nu(-)$ | 0.2866 |
| $\lambda$ (GPa) | 110.7 |
| $\mu$ (GPa) | 82.4 |

The modulus of elasticity and Poisson's ratio are related to the Lame's constants as, $\lambda = \frac{E\nu}{(1-2\nu)(1+\nu)}$ and $\mu = \frac{E}{2(1+\nu)}$. Further, the bulk longitudinal and shear wave velocities can be estimated using the Lame's constants and material density as, $C_L = \sqrt{\frac{\lambda+2\mu}{\rho}}$ and $C_T = \sqrt{\frac{\mu}{\rho}}$. The Lame's constants and the wave velocities are shown in Table.1 and 2 respectively.

Table 2 Wave velocities in the Rail track specimen

| Wave type | Velocity (m/sec) |
|---|---|
| Rayleigh wave | 3008.911 |
| Longitudinal | 5943.487 |
| Shear | 3250.455 |

## 3. Experimental study

### 3.1 The experimental setup

The experimental setup is fully non-contact comprising an actuation laser and a three dimensional (3D) receiving laser. Due to the fact that a raw laser beam will induce multiple wave modes simultaneously into the tested specimen, a slit mask coupled with optics setup arrangement is used to convert the beam into a series of multiple laser lines [5]. This ensures a generation of pure Rayleigh surface wave mode into the specimen and the frequency is determined by the spacing between each laser line as shown in Fig.1. At the receiving end, a 3D scanning laser doppler vibrometer (SLDV) is used to capture the Rayleigh wave propagation exhibiting *x*-, *y*-, and *z*-particle motions. The schematic of the complete experimental setup and the equipment's used in the present study is shown in Fig.1.

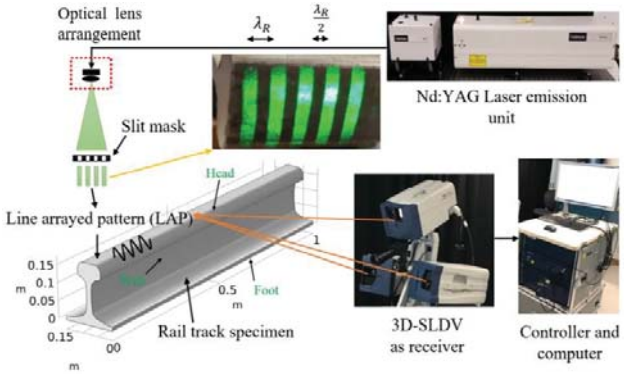


Fig.1 Schematic diagram of high-speed rail track inspection system

The arrangement for scanning the surface of head of specimen is shown in Fig.2. For each measurement, the actuation and reception laser are moved simultaneously along the scanning direction with a fixed distance. Based on the results from the numerous experiments conducted, this distance has been found to be 60 mm for multiple specimens. For this specific distance, the signal is received with less reflections from the edges of the specimen and with higher SNR that is easy to analyze and interpret.

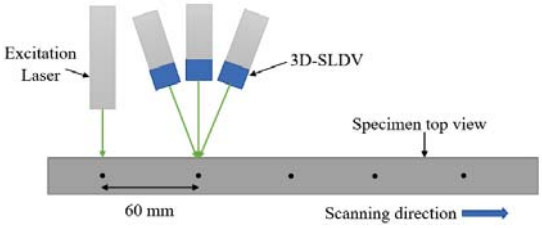


Fig. 2 Schematic of scanning arrangement

## 4. Numerical study

### 4.1 The Finite Element model setup

In order to excite Rayleigh surface waves in the test specimen, a plexiglass wedge is modeled in the simulation as shown in Fig.3. The angle required to excite the Rayleigh wave in the Rail specimen is calculated as the inverse sin of the bulk longitudinal velocity in the plexiglass wedge over the Rayleigh velocity in the rail track specimen [2]. The wedge is modeled at a distance of 190 mm from the nearest end to correlate results with the laboratorty experiments.

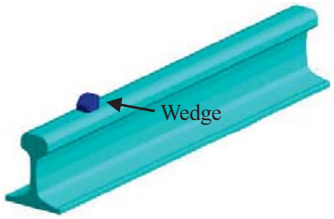


Fig. 3 Schematic diagram of FE model

The excitation applied at the flank of wedge is a 6.5 cycles sine wave modulated with gaussian function and a central frequency of 500 kHz. This applied excitation signal in time and frequency domain is shown in Fig.4. For this frequency of 500 kHz, a penetration depth of around 6 mm can be achieved which is also equal to the wavelength of the Rayleigh wave. Thus, a Rayleigh wave signal launched into the rail track specimen at this frequency could be useful to interrogate the surface damages caused by the rolling contact fatigue [4].

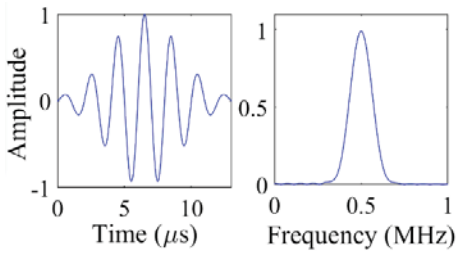


Fig. 4 Excitation signal in time and frequency domain

## 5. Results and Discussions

This section discusses the results obtained from the study. Firstly, the results from an intact specimen are presented. The wave animation over two different time instants for an intact rail track specimen is shown in Fig. 5. It can be seen that the bulk wave excited at the flank of the wedge at a crtical angle of $47.4^0$, generates a pure Rayleigh wave in the specimen which then propagates along the surface.

Fig. 5 Wave propagation showing generation of bulk wave in wedge and Rayleigh wave in Rail track specimen [side view]

Next, the results from experiments at intact state are presented for measurements conducted at different times. As a result of the surface conditions of the specimen as well as the repeatability issues associated with the use of the excitation Laser, the signals received using the laser system at different times are compared to check the variation between each of them. Thus, the repeatability of the experimental results is firstly verified and is presented in Fig.6. It can be seen that certainly there are variations in the measurements – M1, M2, & M3. Thus, an effective signal processing method [5] namely Self adaptive smart algorithm (SASA) was applied to each of the recorded time-domain signals. SASA is based on the concept that a reflection of the incident wave caused by any irregularity (defect) or boundary in the specimen will exhibit almost similar shape of the incident wave and thereby yield a maximum correlation. The details of this developed method can be found in author's previous work [5]. This method is effective in suppressing high levels of noise and leaving behind only the useful wave packets in the time-domain signal after filtering. One of the signals processed with SASA is shown in Fig.6. It can be seen that the filtered signal is now fully free of noise and is dominated by the incident wave packet. There are no any other potential reflections as it is an intact specimen and the excitation and sensing are optimized to minimize the reflections from the specimen boundaries.

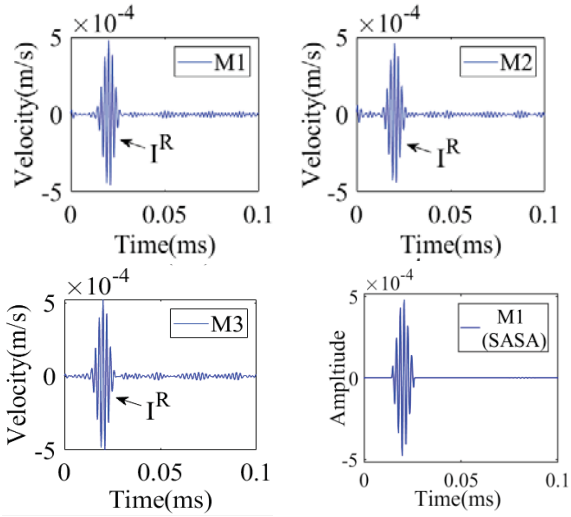


Fig. 6 Time domain responses for intact sample and SASA filtering

Next, a defect is artifically created on the specimen surface at a distance of 350 mm from the near end as shown in Fig.7. The distance between excitation (E) and sensing (S) is fixed at 60 mm throuhgout the measurements. A line scanning was conducted and the results for B-scan constructed from the measurements at different location versus time is shown in Fig.8. The line consists of 77 sensing points with a uniform distance between each sensing point 1.6 mm. Thus, the total length of the line is 123.2 mm.

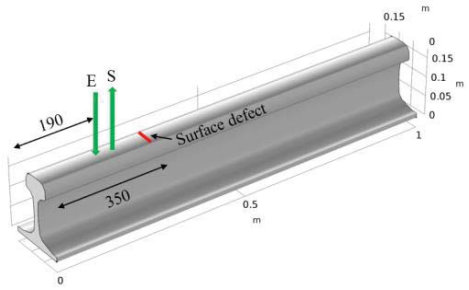


Fig. 7 Schematic of excitation, sensing & defect location

It can be seen that there is a incident wave packet as well as a defect wave packet propagating in the specimen. Besides, it is well observed that as soon as the incident wave encounters the surface defect, there is a sudden loss of energy due to blockage by the defect and this wave energy is reflected back towards the source as highlighted by the defect reflected wave in Fig.8. It is also observed that a few scanning points receive a time-domain signal that has an inconsistent trend and not in proportion to the other received waveforms. This behavior is highlighted by a red ellipse as shown in Fig.8 and can be better tackled with the SASA technique. Further, two sample time domain waveforms are shown in Fig.9 (a) and (b) when the distance between E and S is 60 mm. It can be seen that both the signals are quite easy to analyse and interpret.

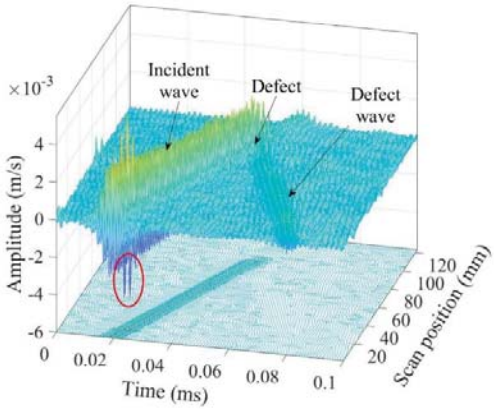


Fig. 8 B-scan result of the line scanning measurements

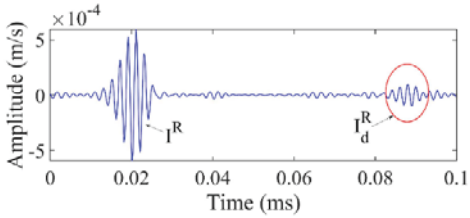


(a) Ext-End: 190 mm; Ext-Sensing: 60 mm; Ext-Defect: 160

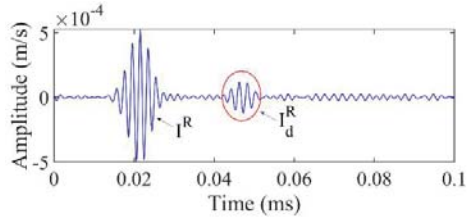


(b) Ext-End: 250 mm; Ext-Sensing: 60 mm; Ext-Defect: 40

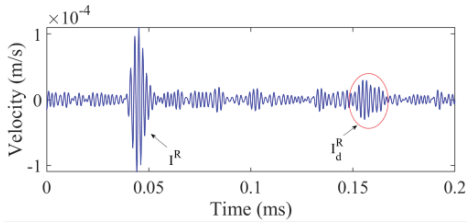


(c) Ext-Sensing: 130 mm; Ext-Defect: 715 mm

Fig. 9 Time-domain waveforms of continuous scanning along the Rail specimen

It can be seen from Fig.9(c), when the distance between excitation to sensing is increased more than 60 mm, the signal consists of many wave packets, perhaps noise, and the defect reflected signal could be deceived as a noise too. It is therefore paramount to select a proper excitation and reception strategy that could help to receive good quality signals without ending up yielding faulty alarm with respect to defect detection in the rail tack specimen. Lastly, a 3D finite element simulation was conducted with the same settings as described for the experimental measurements. The results from the simulation very well correspond to the experiments as shown in Figs. 6, 9(a), and 10.

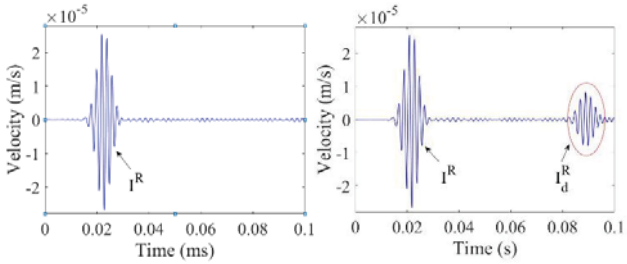


Fig. 10 Time domain waveforms from simulation studies (a) Intact (b) Ext-End: 190 mm; Ext-Sensing: 60 mm; Ext-Defect: 160

## 6. Conclusions

The present study focusses on investigating the surface structural integrity of rail track specimen using a fully non-contact optical system. Rayleigh waves were actuated and sensed at different locations on the specimen surface. After selecting a proper actuation and reception strategy, the recorded signals were found to be easy to analyze and interpret. The results show that proposed inspection system and the strategy found after conducting multiple experiments can be helpful for inspecting rail track specimens in a completely non-contact manner with reasonably good accuracy.

## ACKNOWLEDGEMENT

This work is partially supported by the Agency for Science, Technology and Research (A*STAR), Singapore, under the RIE2020 AME Industry Alignment Fund - Prepositioning Programme (IAF-PP) (Grant number: A19C9a0044, A20F5a0043).

## REFERENCES

1. Kim, N.H., Sohn, H. and Han, S.W., "Rail inspection using noncontact laser ultrasonics," Journal of the Korean Society for Nondestructive Testing, Vol. 32, No. 6, pp.696-702, 2012.
2. Masurkar, F., Yelve, N.P. and Tse, P., "Nondestructive testing of rails using nonlinear Rayleigh waves," Proceedings of the Institution of Mechanical Engineers, Part C: Journal of Mechanical Engineering Science, Vol. 203-210, 2022.
3. Heckel, T., Wack, Y. and Mook, G., 2019. Simulation of an instrumented ultrasonic test run with a rail inspection train. Review of Progress in Quantitative Nondestructive Evaluation.
4. Masurkar, F., Ming Ng, K., Tse, P.W. and Yelve, N.P., "Interrogating the health condition of rails using the narrowband Rayleigh waves emitted by an innovative design of non-contact laser transduction system," Structural Health Monitoring, 2020.
5. Masurkar, F., Rostami, J. and Tse, P., "Design of an innovative and self-adaptive-smart algorithm to investigate the structural integrity of a rail track using Rayleigh waves emitted and sensed by a fully non-contact laser transduction system," Applied Acoustics, 166, 2020.